

FeRh metamagnetic and martensitic transformations and the ground-state structure

Nikolai A. Zarkevich^{1,*} and D. D. Johnson^{1,2,†}

¹Ames Laboratory, U.S. Department of Energy, Ames, Iowa 50011 USA

²Departments of Materials Science & Engineering, Iowa State University, Ames, Iowa 50011 USA

(Dated: July 23, 2022)

FeRh is a showcase for caloric materials genome, transforming upon heating from the type-2 antiferromagnet (AFM) to a ferromagnet (FM). FeRh AFM (but not FM) cubic B2 lattice is unstable at ambient pressure. We describe the stable orthorhombic AFM FeRh structure at low temperature T . We claim that the austenitic AFM B2 phase has a premartensitic instability at room T , and it must transform to a martensite at cryogenic T below ~ 23 K. We also address the metamagnetic phase transformation at $T_c = 353$ K and detail contributions to the caloric effect.

Keywords: FeRh, ground state, caloric, phase transformation

INTRODUCTION

FeRh reveals surprising properties even after extensive experimental [1–21] and theoretical [22–35] studies. Fe–Rh alloys could find use in caloric [12, 13, 20, 36–39] and nanoscale devices [21, 35, 40–47]. Precious Rh is produced mostly in South Africa and Russia [48] and priced from 9.7×10^4 in 2010 to 3.1×10^4 USD/kg in 2015 [49], hence its bulk use is prohibitively expensive, while thin-film and nanoscale applications can be practical.

The B2 (cP2, CsCl-type) FeRh exhibits transformation between the low-T anti-ferro-magnetic (AFM) and high-T ferromagnetic (FM) phases (Fig. 3) around $T_c = 353$ K, with a large 12% density decrease [9, 12]. T_c lowers with increasing at.% Rh in the off-stoichiometric samples [5]. FeRh shows magneto-, elasto-, and baro-caloric effects and a large entropy change ΔS at the metamagnetic AFM–FM phase transition. Experiment [12] shows a large temperature drop (12.9 K at 1.95 Tesla) in the quenched $\text{Fe}_{49}\text{Rh}_{51}$ sample.

We find that B2 structure with AFM (but not FM) ordering is unstable at ambient pressure, in agreement with recent reports [34, 35]. The stable AFM structure is orthorhombic (Fig. 1), but its energy is only a few meV/atom below that of an ideal cubic B2 structure (Fig. 2); this energy difference is too small compared to $k_B T_c = 30$ meV at $T_c = 353$ K (here k_B is the Boltzmann constant). Due to higher entropy (Fig. 4), the more symmetric cubic B2 structure has lower Gibbs free energy at ambient T . Indeed, the experimentally observed AFM structure at room T is a cubic austenite [5, 15, 50]. We expect that FeRh should transform to a martensite at a cryogenic T below ~ 23 K.

RESULTS

Stable AFM orthorhombic structure

What is the stable structure of FeRh at low T ? To find it, we constructed a set of large supercells with the type-2

AFM ordering of the atomic magnetic moments (Fig. 3d). Next, using *ab initio* molecular dynamics within DFT, we equilibrated each supercell at high T (chosen in the range between 353 and 1000 K), cooled it to 0 K, after that (using the conjugate gradient method in DFT) fully relaxed the obtained structures, keeping the AFM spin ordering. We found that the final structure (Fig. 1) has a lower energy than the ideal AFM B2, although the energy difference is only a few meV/atom (Fig. 2). The phonon (Fig. 9) and NEB calculations (Fig. 2) confirm that this orthorhombic AFM structure is stable.

Most of the supercell calculations converged to the same orthorhombic structure with or without planar defects, consistent with formation of a martensite. Again, for a number of different supercells this final structure was the same, with the orthorhombic primitive cell (Fig. 1) having $Pmmn$ space group #59. This D_{2h} $Pmmn$ symmetry group of electronic and atomic order accounts for different orientations of Fe magnetic moments in the AFM structure (Fig. 3f), while the space group for the atomic ordering (ignoring the spin structure) would be C_{2v} $Pmma$ #51. The orthorhombic structure can be viewed as a monoclinic (see Fig. 1 and

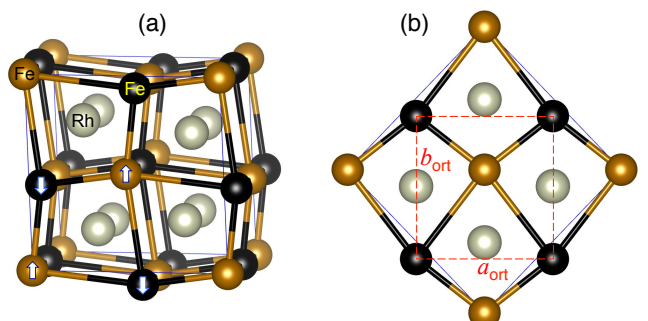


FIG. 1. The stable orthorhombic AFM structure of FeRh (a) and its 001 projection (b). Magnetic moment of Rh (white) is zero. Fe magnetic moments are directed up (golden) and down (black). The lattice vectors of the orthorhombic primitive cell (red dashed lines) are oriented along the cubic [110], $[\bar{1}10]$, and [001] directions.

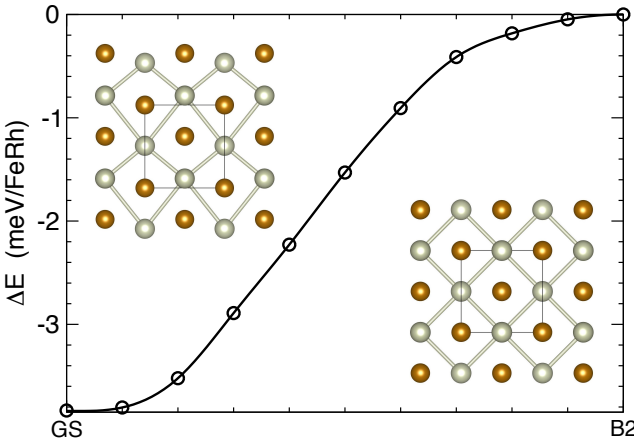


FIG. 2. The minimal enthalpy path from B2 to the orthorhombic ground-state (GS) structure has no barrier. The insets show the orthorhombic (upper left) and the cubic B2 (lower right) structures in the 001 projection, with vertical and horizontal axes along the cubic [110] and $[\bar{1}10]$ directions. Fe is golden yellow; Rh is white. Rh-Rh bonds are thick white. The orthorhombic unit cell is shown by thin black lines.

Fig. 5 in [35]) with a twice larger unit cell. However, the orthorhombic space group differs from the monoclinic $P2/m$, suggested in [35].

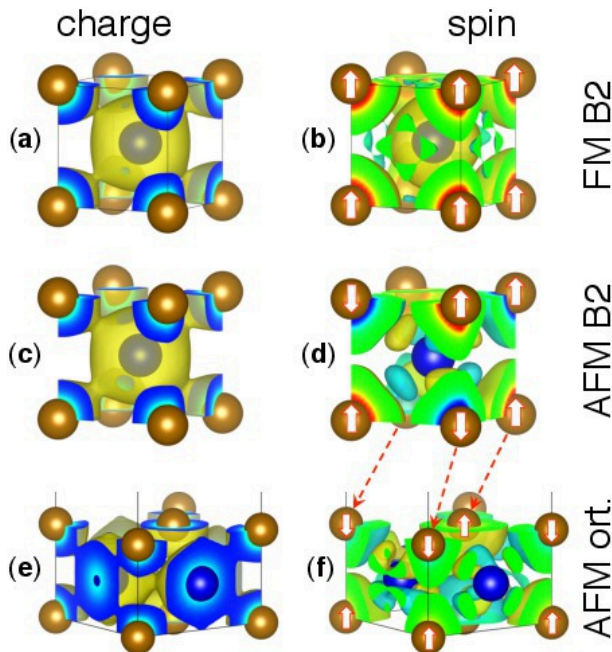


FIG. 3. Electronic (a,c,e) and spin (b,d,f) density (with 0.046 and $0.002 e/\text{\AA}^3$ iso-surfaces, respectively) in FeRh FM B2 (a,b), AFM B2 (c,d), and AFM orthorhombic (e,f) structures. Fe (Rh) atoms are golden (dark blue).

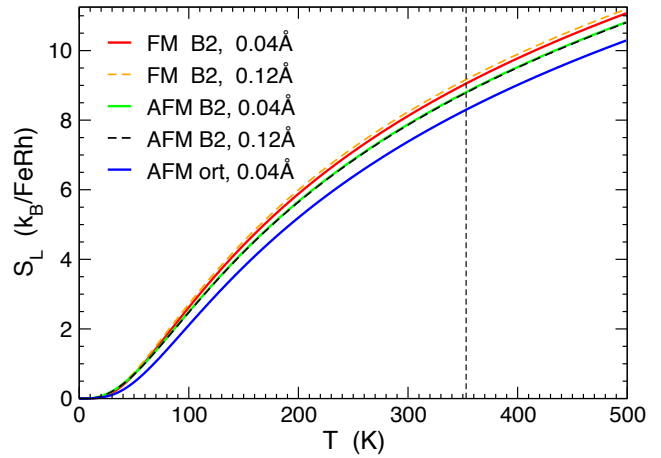


FIG. 4. Lattice entropy S_L , calculated using the phonon code [51] for the fully relaxed FM B2, AFM B2, and AFM orthorhombic structures at $P=0$, using small (0.04 Å) and large (0.12 Å) atomic displacements.

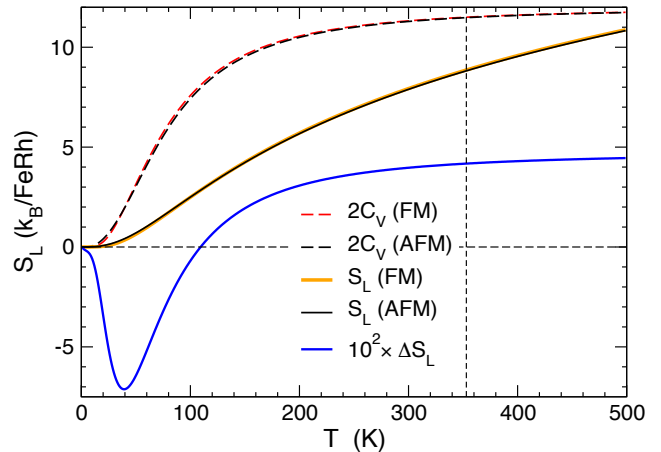


FIG. 5. Lattice entropy S_L and heat capacity C_V of FM and AFM B2 structures, calculated at the same $a = 2.997$ Å, using small (0.04 Å) atomic displacements [51].

Martensitic transformation at cryogenic T

The solid-state NEB [52, 53] calculations find no energy barrier for the martensitic transformation between cubic B2 and orthorhombic AFM structures, see Fig. 2.

We predict that at a cryogenic $T \sim 23$ K the AFM cubic B2-type austenite transforms to a martensite of the orthorhombic structure, shown in Fig. 1. The transformation is martensitic, without diffusion. The orthorhombic structure is lower in energy than B2, but only by a few meV/atom. The expected martensitic transformation temperature T_m is of the order of tens Kelvins; it can be further suppressed by the martensitic stress [54].

Although the cubic B2-type AFM austenite is stabilized by entropy at room T , it should have a pre-martensitic instability, similar to that in the B2-type

NiTi austenite [55, 56]. Its anomalous structural behavior is predicted by phonon (Fig. 8) and NEB (Fig. 2) calculations and confirmed by experiment [18].

Metamagnetic transformation near 353 K

The calculated energy difference between (unstable) AFM and (stable) FM B2 fully relaxed structure at zero pressure is $\delta E_0 = 29.8$ meV/atom, see Fig. 6, and compares well with previous calculations [25]. The estimate (eq. 3.7 on page 33 in [57]) provides $T_c = \delta E_0/k_B = 346$ K, while the experimental value is around 353 K (80°C) for the Fe₅₀Rh₅₀ sample [5]. This estimate is applicable not only to the stoichiometric FeRh at 50 at.% Rh, but also to partially disordered samples with off-stoichiometric composition. From the electronic density of states (DOS) in Fig. 7, we expect that lowering of the Fermi energy (for example, due to decrease in %Rh) will stabilize the FM phase, with a lesser effect on the AFM phase. This will decrease the energy difference between the FM and AFM phases, and must reduce T_c . Indeed, this theoretical expectation agrees with the experimental phase diagram [5, 15, 50].

The AFM to FM transformation is magnetostructural: it is accompanied by changes of electronic structure and volume. We remind that the electronic transformation happens with the speed of light c_{light} , while the structural transformation (including volume change) propagates not faster than with the speed of sound $v_{sound} \ll c_{light}$ [54]. The electronic transformation is accompanied by discontinuity in pressure, which drives the volume change [53]. From the other hand, possible causes for the electronic transformation include initial structure change or application of an external field. In particular, the magnetostructural transformation of FeRh can be caused by an application of an external magnetic field or stress (or their combination) or by thermal expansion.

Thermal expansion

We calculate energy versus volume (Fig. 6) and use eq. A1 in [58] to estimate the linear thermal expansion in the stable FM phase. We get $\alpha_L = 6.5 \times 10^{-6} \text{ K}^{-1}$, in agreement with the measured values of $6.7 \pm 0.3 \times 10^{-6} \text{ K}^{-1}$ [9] and $6 \times 10^{-6} \text{ K}^{-1}$ [59].

However, for the AFM B2 structure the calculated [58] ($6.5 \times 10^{-6} \text{ K}^{-1}$) and experimental [9] ($9.5 \times 10^{-6} \text{ K}^{-1}$) values differ by 46%. This disagreement indicates that the experimental structure is not precisely B2. Indeed, AFM B2 structure is unstable, while the suggested stable AFM structure is orthorhombic (Fig. 1), and its calculated linear thermal expansion coefficients along a , b , and c axes are 14, 16, and $21 \times 10^{-6} \text{ K}^{-1}$, respectively.

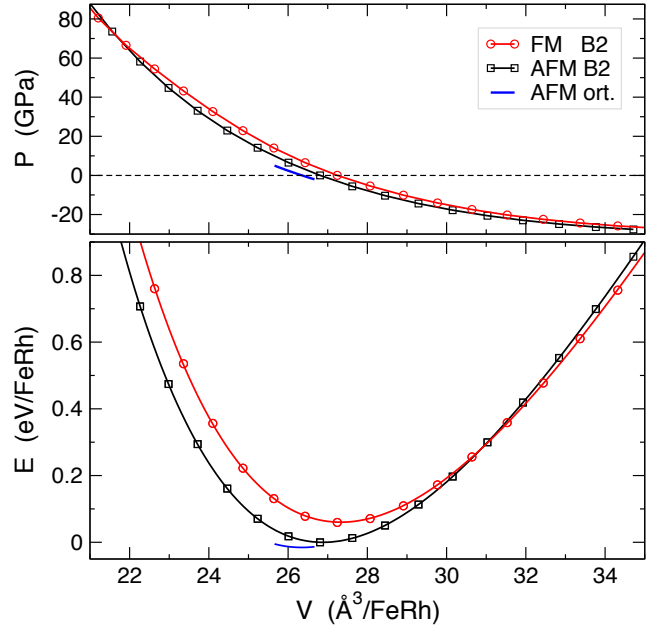


FIG. 6. Energy E (eV/f.u.) and pressure P (GPa) vs. volume V (Å/f.u.) for FM B2, AFM B2, and AFM GS structures.

The averaged uniform linear thermal expansion for the martensite of the orthorhombic phase is $17 \times 10^{-6} \text{ K}^{-1}$.

The austenitic cubic B2 phase has a premartensitic instability. Its structure at room T is neither ideal B2 nor the stable orthorhombic. As expected, its measured linear thermal expansion coefficient of $9.5 \times 10^{-6} \text{ K}^{-1}$ is between the calculated values of $6.5 \times 10^{-6} \text{ K}^{-1}$ for the unstable ideal B2 and $17 \times 10^{-6} \text{ K}^{-1}$ for the martensite.

The estimate [58] ignores internal atomic motion. This approximation is acceptable for the stable FM phase, but not for the AFM B2 FeRh. To address the AFM phase, taking into account atomic motion, we calculate phonon entropy at two lattice constants and use the equation $(\partial S/\partial V)_P/K = \alpha_V$, where $K = -V(dP/dV) = -V(d^2E/dV^2)$ is the bulk modulus and $\alpha_V \approx 3\alpha_L$ is the volumetric thermal expansion. From $E(V)$ dependence in Fig. 6 we find $K \approx 200 \text{ GPa}$ ($1.25 \text{ eV}/\text{\AA}^3$), while the lattice entropy at 353 K is $7.68 k_B/\text{FeRh}$ at $a = 2.887 \text{ \AA}$ and $8.82 k_B/\text{FeRh}$ at 2.997 \AA , hence $(\partial S/\partial V) = 0.4 k_B/\text{\AA}^3$, $\alpha_V = 2.75 \times 10^{-5} \text{ K}^{-1}$ and $\alpha_L = 9.2 \times 10^{-6} \text{ K}^{-1}$, which compares well with $\alpha_L^{Expt} = 9.5 \times 10^{-6} \text{ K}^{-1}$ from experiment [9].

Premartensitic instability in the AFM B2 phase

Instability of the AFM B2 structure is revealed by phonon (Fig. 8) and NEB (Fig. 2) calculations and confirmed by experiment [18]. This instability explains deviation of the calculated equilibrium lattice constants a_0 and thermal expansion from experiment. Indeed, the cal-

culated values of a_0 at zero pressure are 2.996 Å and 3.012 Å in the AFM and FM B2 phases, respectively, while the experimental measurements at 353 K (80°C) give 2.887 Å and 2.997 Å for the FeRh sample at 50.0 at.%Rh [9] (similar to earlier measurement [6]); they agree (within 0.5%) for the FM, but not the AFM B2 phase.

Electronic structure

The iso-surfaces of electronic and spin density around Fe and Rh atoms are shown in Fig. 3. Due to symmetry, the spin density around Rh atom sums to zero atomic magnetic moment in the AFM structures, see Fig. 3(d,f).

The calculated electronic density of states $n(E)$ in Fig. 7 agrees with recent calculations (Fig. 6 in [35], Fig. 4 in [34], Fig. 2 in [33], Fig. 1 in [30]). Comparing the total DOS at the Fermi level $n(E_F)$ in the FM and AFM states, one can see that it changes substantially during the AFM–FM phase transformation. This explains a large contribution of electronic entropy to the total entropy change $\Delta S_T(T_c)$.

The electronic DOS at the Fermi level $n(E_F)$ is 2.310 and 0.677 states eV⁻¹ per FeRh formula unit in the FM and AFM phases. The electronic entropy, estimated using the Sommerfeld expansion, is $S_e \approx (\pi^2/3) \cdot k_B^2 T \cdot n(E_F) = 0.23$ and 0.07 k_B /FeRh in the FM and AFM phases, respectively. The difference $\Delta S_e = 0.163 k_B$ /FeRh (or 0.08 k_B per atom) is the leading con-

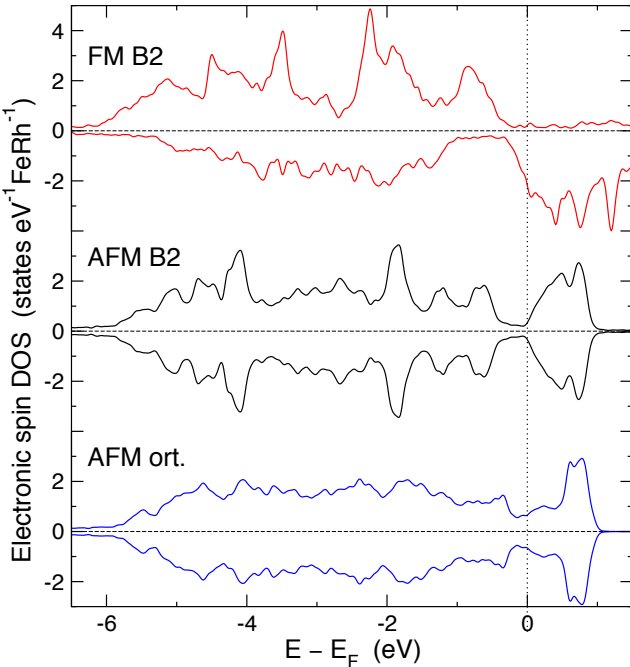


FIG. 7. Electronic DOS of the ideal cubic B2 structure with FM (upper) and AFM (middle) spin ordering, and the AFM orthorhombic structure (lower) at $P=0$.

tribution to the total ΔS_T , in agreement with prediction of Ponomarev [22] and its recent confirmation [29].

Phonons

The AFM B2 FeRh is known to have unstable phonons [35]. Using the small displacement method [51] at zero pressure P , we find an unstable phonon mode at M (110) in the type-2 AFM B2 phase, but not in the FM phase (Fig. 8), in agreement with recent calculations [34]. We remind that soft phonon modes affect the lattice entropy S_L . The large displacement method within the quasi-harmonic approximation (QHA) is just a computational trick to avoid the unstable phonons and find the lattice entropy S_L (see Fig. 4). This T -dependent entropy is calculated at the phase-specific fixed lattice constants $a_0(P=0, T=0)$, ignoring the thermal expansion.

Interestingly, we find that the calculated lattice entropy of the FM phase strongly depends on the chosen atomic displacement d , changing from $8.859 k_B$ /FeRh for small $d = 0.04$ Å to $8.972 k_B$ /FeRh for large $d = 0.12$ Å at fixed $a = 2.997$ Å. In the AFM phase, we find a small change from 8.8176 to $8.7945 k_B$ /FeRh for the same displacements. The values from the small displacement method ($d = 0.04$ Å) give a rather small $\Delta S_L = 0.042 k_B$ /FeRh (or $0.02 k_B$ per atom).

Our calculations indicate that at ambient conditions the FM FeRh phase is stable, but not harmonic. For the least harmonic phonons, frequency dependence on the atomic displacement d is the strongest. The high-frequency optical phonon modes are harmonic in both FM and AFM phases, while the low-frequency acoustic phonons show less harmonic behavior around M , where the difference between modes, calculated for $d = 0.04$ and 0.12 Å (red and black lines in Fig. 8), is the largest.

To calculate phonons at a given T , one could use results from an *ab initio* molecular dynamics at that T in the ThermoPhonon code [55, 60]. We leave this exercise beyond the scope of the present paper, because the leading contribution to the total entropy change is electronic.

Entropy

The total entropy has the lattice (L), electronic (e), and magnetic (m) contributions: $S = S_L + S_e + S_m$. We calculate entropy change $\Delta S = S(FM) - S(AFM)$ due to electronic transformation at $T_c = 353$ K at fixed lattice constant $a = 2.997$ Å (measured [9] in the Fe₅₀Rh₅₀ FM phase at T_c). Neglecting the magnetic entropy change, which is a difference of rather small values of S_m in the fully ordered FM and AFM phases, we get the total entropy change $\Delta S_T = 0.103 k_B$ per atom (or $11 \text{ J kg}^{-1} \text{K}^{-1}$) for the electronic transformation at T_c at constant volume V . Experiments provide the assessed

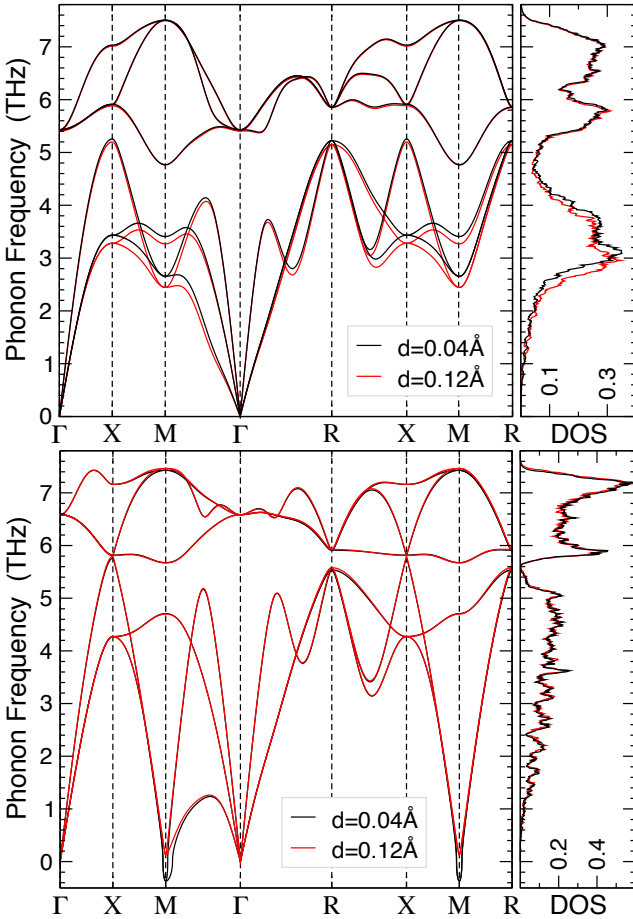


FIG. 8. Phonon frequencies and DOS for FeRh FM B2 (upper) and AFM B2 (lower) structures, calculated using small (0.04\AA) and large (0.12\AA) atomic displacements d . The AFM B2 structure has an unstable phonon mode at $M(\frac{1}{2}, \frac{1}{2}, 0)$.

values of ΔS_T ranging from 12 to 14 J/(kg K) [8, 20, 38], depending on the assessment method [20] and sample composition [8] and preparation [12]. The early theoretical estimate [22] was $\Delta S_T = 18.3 \text{ J kg}^{-1}\text{K}^{-1}$ and $\Delta T_S = -T_c \Delta S_T / C_B = -(20 \pm 2) \text{ K}$ for the temperature change at constant entropy. Here $C_B(B, T)$ is the heat capacity at constant magnetic field B .

Using $C_B \approx C_V \approx 3k_B/\text{atom}$ (or $314 \text{ J kg}^{-1}\text{K}^{-1}$) for solid FeRh at $T \geq 300 \text{ K}$ (see Fig. 5), we quickly find the maximal isoentropic temperature change $\Delta T_S = -T_c \Delta S_T / C_B = -12.1 \text{ K}$. It agrees well with the experimental [20] estimates, ranging from -10.6 to -12 K .

The assessed ΔT_S should not be confused with the adiabatic temperature change $\Delta T_{ad}(\Delta B)$, produced by added external field ΔB , such as directly measured at $\Delta B = 1.95 \text{ Tesla}$ caloric effect $\Delta T_{ad} = 3.8 \text{ K}$ (12.9 K) for the annealed (quenched) Fe₄₉Rh₅₁ samples [12].

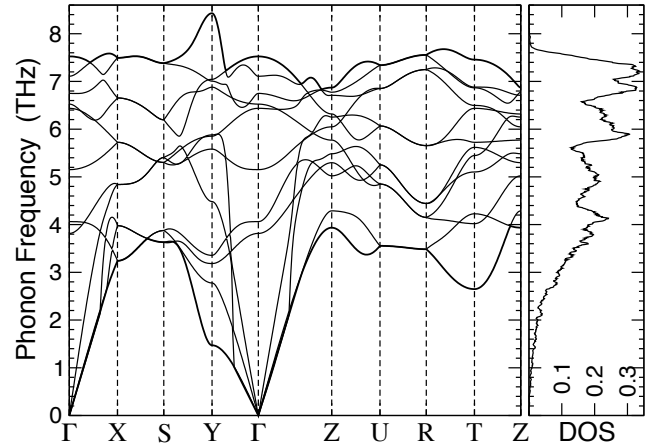


FIG. 9. Phonon frequencies and DOS for AFM orthorhombic structure, calculated using small (0.04\AA) displacements.

Estimate of dT_c/dH

The calculated magnetization of the fully relaxed AFM and FM FeRh B2 structures is 0 and $2.1\mu_B/\text{atom}$, respectively. Using the upper bound for the magnetization change $\Delta M(T_c) < [M(\text{FM}) - M(\text{AFM})]$ during the AFM–FM transformation, we find $-dT_c/dH = \Delta M/\Delta S_T < 2.1\mu_B/0.103k_B = 13.7 \text{ K/Tesla}$, while the value of $\Delta M(T_c)$ at 60% of this upper estimate provides $-dT_c/dH = 8.2 \text{ K/T}$ for the stoichiometric FeRh. Measurements of T_c in the external magnetic field H (or critical field H_c vs. T) provide a quadratic [10] dependence with the linear [6] slope $-dT_c/dH$ in small fields of 8.2 in FeRh [8]; 8.2 in Fe_{49.5}Rh_{50.5} [19]; 8.5 in Fe₄₉Rh₅₁ [20]; and from 9.6 to 9.7 K/Tesla [38] in Fe₄₉Rh₅₁.

SUMMARY

We confirm that the AFM cubic B2 FeRh structure is unstable, suggest the stable low- T orthorhombic structure, and predict a martensitic transformation within the AFM FeRh phase at cryogenic temperature. A structural instability in one of the phases is a necessary (but not sufficient) condition for zero enthalpy barrier and small hysteresis, needed for caloric cooling. In addition, we predict the linear thermal expansion coefficients, the bulk modulus, the transition temperature, as well as entropy and temperature change at the caloric transformation, and find agreement with experiment. We look forward to experimental verification of the predicted FeRh martensite.

This work was supported by the U.S. Department of Energy (DOE), Office of Science, Basic Energy Sciences, Materials Science and Engineering Division. Ames Laboratory is operated by Iowa State University under contract DE-AC02-07CH11358.

Computational Details

DFT calculations were performed using the modified VASP code [61, 62] with built-in C2NEB algorithm [63, 64]. We used the projector augmented waves (PAW) [65, 66] and PBE exchange-correlation functional [67] with Vosko-Wilk-Nusair spin-polarisation [68]. We used the modified Broyden method [69] for accelerating convergence. The Brillouin zone integration was performed on a dense Monkhorst-Pack mesh [70] with ≥ 50 k -points per \AA^{-1} , including Γ . The cut-off energy for the plane wave basis set was increased to 334.9 eV (and 511.4 eV for the augmentation charge) by the high-precision flag.

Phonons were calculated using the Phon code [51]. The atomic displacements varied from 0.04 to 0.12 \AA in a cubic $4 \times 4 \times 4$ supercell containing 64 FeRh formula units (128 atoms). An additional, third support grid was used for the evaluation of the augmentation charges in DFT.

The nudged elastic band method without climbing (preserved in the C2NEB code [64]) was used to find the transformation without enthalpy barrier in Fig. 2.

-
- * zarkev@ameslab.gov
† ddj@ameslab.gov
- [1] M. Fallot, Ann. Phys. (Paris) **10**, 291 (1938).
 - [2] M. Fallot, Rev. Sci. **77**, 498 (1939).
 - [3] F. de Bergevin and L. Muldawer, Compt. Rend. **252**, 1347 (1961).
 - [4] J. S. Kouvel and C. C. Hartelius, J. Appl. Phys. **33**, 1343 (1962).
 - [5] G. Shirane, C. W. Chen, P. A. Flinn, and R. Nathans, Phys. Rev. **131**, 183 (1963).
 - [6] A. Zakharov, A. Kadomtseva, R. Levitin, and E. Pomyatovskii, Soviet Physics JETP **19**, 1348 (1964), translated from: J. Exptl. Theoret. Phys. (ZhETF) **46** (6), 2003–2010 (1964).
 - [7] G. Shirane, R. Nathans, and C. W. Chen, Phys. Rev. **134**, A1547 (1964).
 - [8] J.S. Kouvel, J. Appl. Phys. **37**, 1257 (1966).
 - [9] L. Zsoldos, Physica Status Solidi (B) **20**, K25 (1967).
 - [10] J. B. McKinnon, D. Melville, and E. W. Lee, J. Phys. C: Solid State Physics **3**, S46 (1970).
 - [11] L. Vinokurova, A. Vlasov, N. Kulikov, and M. Pardavi-Horváth, J. Magn. Magn. Mater. **25**, 201 (1981).
 - [12] S. Nikitin, G. Myalikgulyev, A. Tishin, M. Annaorazov, K. Asatryan, and A. Tyurin, Physics Letters A **148**, 363 (1990).
 - [13] M. Annaorazov, K. Asatryan, G. Myalikgulyev, S. Nikitin, A. Tishin, and A. Tyurin, Cryogenics **32**, 867 (1992).
 - [14] M. P. Annaorazov, S. A. Nikitin, A. L. Tyurin, K. A. Asatryan, and A. K. Dovletov, J. Appl. Phys. **79**, 1689 (1996).
 - [15] J. Balun, L. Eleno, and G. Inden, Intermetallics **15**, 1237 (2007).
 - [16] S. Inoue, H. Yu Yu Ko, and T. Suzuki, IEEE Trans. Magnetics **44**, 2875 (2008).
 - [17] I. Radu, C. Stamm, N. Pontius, T. Kachel, P. Ramm, J.-U. Thiele, H. A. Dürr, and C. H. Back, Phys. Rev. B **81**, 104415 (2010).
 - [18] Y. Wakisaka, Y. Uemura, T. Yokoyama, H. Asakura, H. Morimoto, M. Tabuchi, D. Ohshima, T. Kato, and S. Iwata, Phys. Rev. B **92**, 184408 (2015).
 - [19] R. Onodera, K. Ohtake, K. Takahashi, S. Kimura, K. Watanabe, and K. Koyama, J. Japan Inst. Met. Mater. **80**, 186 (2016).
 - [20] A. Chirkova, K. Skokov, L. Schultz, N. Baranov, O. Gutfleisch, and T. Woodcock, Acta Materialia **106**, 15 (2016).
 - [21] F. Pressacco, V. Uhl, M. Gatti, A. Bendounan, E. E. Fullerton, and F. Sirotti, Scientific Reports **6**, 22383 (2016).
 - [22] B.K. Ponomarev, Soviet Physics JETP **36**, 105 (1973), translated from Zh. Eksp. Teor. Fiz. 63, 199–204 (1972).
 - [23] N.P. Grazhdankina, Soviet Physics Uspekhi **11**, 727 (1969).
 - [24] H. Hasegawa, J. Magn. Magn. Mater. **66**, 175 (1987).
 - [25] V. L. Moruzzi and P. M. Marcus, Phys. Rev. B **46**, 2864 (1992).
 - [26] V. L. Moruzzi and P. M. Marcus, Phys. Rev. B **46**, 14198 (1992).
 - [27] C. Paduani, J. Appl. Phys. **90**, 6251 (2001).
 - [28] L. M. Sandratskii and P. Mavropoulos, Phys. Rev. B **83**, 174408 (2011).
 - [29] J. B. Staunton, R. Banerjee, M. d. S. Dias, A. Deak, and L. Szunyogh, Phys. Rev. B **89**, 054427 (2014).
 - [30] J. Kudrnovský, V. Drchal, and I. Turek, Phys. Rev. B **91**, 014435 (2015).
 - [31] E. Mendive-Tapia and T. Castán, Phys. Rev. B **91**, 224421 (2015).
 - [32] J. Barker and R. W. Chantrell, Phys. Rev. B **92**, 094402 (2015).
 - [33] S. Polesya, S. Mankovsky, D. Ködderitzsch, J. Minár, and H. Ebert, Phys. Rev. B **93**, 024423 (2016).
 - [34] U. Aschauer, R. Braddell, S. A. Brechbühl, P. M. Derlet, and N. A. Spaldin, Phys. Rev. B **94**, 014109 (2016).
 - [35] M. Wolloch, M. E. Gruner, W. Keune, P. Mohn, J. Redinger, F. Hofer, D. Suess, R. Podloucky, J. Landers, S. Salamon, F. Scheibel, D. Spoddig, R. Witte, B. Roldan Cuenya, O. Gutfleisch, M. Y. Hu, J. Zhao, T. Toellner, E. E. Alp, M. Siewert, P. Entel, R. Pentcheva, and H. Wende, Phys. Rev. B **94**, 174435 (2016).
 - [36] M. Manekar and S. B. Roy, J. Phys. D: Applied Physics **41**, 192004 (2008).
 - [37] K. G. Sandeman, Scripta Materialia **67**, 566 (2012).
 - [38] E. Stern-Taulats, A. Planes, P. Lloveras, M. Barrio, J.-L. Tamarit, S. Pramanick, S. Majumdar, C. Frontera, and L. Mañosa, Phys. Rev. B **89**, 214105 (2014).
 - [39] Y. Liu, L. C. Phillips, R. Mattana, M. Bibes, A. Barthélémy, and B. Dkhil, Nature Communications **7**, 11614 (2016).
 - [40] J.-U. Thiele, S. Maat, and E. E. Fullerton, Appl. Phys. Lett. **82**, 2859 (2003).
 - [41] G. Ju, J. Hohlfeld, B. Bergman, R. J. M. van de Veerdonk, O. N. Mryasov, J.-Y. Kim, X. Wu, D. Weller, and B. Koopmans, Phys. Rev. Lett. **93**, 197403 (2004).
 - [42] J. U. Thiele, S. Maat, J. L. Robertson, and E. E. Fullerton, IEEE Transactions on Magnetics **40**, 2537 (2004).
 - [43] R. Fan, C. J. Kinane, T. R. Charlton, R. Dorner, M. Ali, M. A. de Vries, R. M. D. Brydson, C. H. Marrows, B. J.

- Hickey, D. A. Arena, B. K. Tanner, G. Nisbet, and S. Langridge, Phys. Rev. B **82**, 184418 (2010).
- [44] R. O. Cherifi, V. Ivanovskaya, L. C. Phillips, A. Zobelli, I. C. Infante, E. Jacquet, V. Garcia, S. Fusil, P. R. Briddon, N. Guiblin, A. Mougin, A. A. Ünal, F. Kronast, S. Valencia, B. Dkhil, A. Barthélémy, and M. Bibes, Nat. Mater. **13**, 345 (2014).
- [45] X. Marti, I. Fina, C. Frontera, J. Liu, P. Wadley, Q. He, R. J. Paull, J. D. Clarkson, J. Kudrnovsky, I. Turek, J. Kunes, D. Yi, J.-H. Chu, C. T. Nelson, L. You, E. Arenholz, S. Salahuddin, J. Fontcuberta, T. Jungwirth, and R. Ramesh, Nat. Mater. **13**, 367 (2014).
- [46] Z. Q. Liu, L. Li, Z. Gai, J. D. Clarkson, S. L. Hsu, A. T. Wong, L. S. Fan, M.-W. Lin, C. M. Rouleau, T. Z. Ward, H. N. Lee, A. S. Sefat, H. M. Christen, and R. Ramesh, Phys. Rev. Lett. **116**, 097203 (2016).
- [47] X. Zhou, F. Matthes, D. E. Brugler, and C. M. Schneider, AIP Advances **6**, 015211 (2016).
- [48] V. V. Cherdynsev, *Abundance of Chemical Elements* (University of Chicago Press, Chicago, 1961) translated from Russian (GosTechIzdat, Moscow, 1956).
- [49] U.S. Geological Survey, “Mineral commodity summaries,” <https://minerals.usgs.gov/minerals/pubs/commodity/platinum/mcs-2016-plati.pdf> (2016).
- [50] L. Swartzendruber, Bulletin of Alloy Phase Diagrams **5**, 456 (1984).
- [51] D. Alfè, Computer Physics Communications **180**, 2622 (2009).
- [52] D. Sheppard, P. H. Xiao, W. Chemelewski, D. D. Johnson, and G. Henkelman, J. Chem. Phys. **136**, 074103 (2012).
- [53] N. A. Zarkevich and D. D. Johnson, J. Chem. Phys. **143**, 064707 (2015).
- [54] N. A. Zarkevich and D. D. Johnson, Physical Review B **91**, 174104 (2015).
- [55] N. A. Zarkevich and D. D. Johnson, Phys. Rev. B **90**, 060102 (2014).
- [56] N. A. Zarkevich and D. D. Johnson, Phys. Rev. Lett. **113**, 265701 (2014).
- [57] N. A. Zarkevich, *First-principles prediction of thermodynamics and ordering in metallic alloys*, Ph.D. thesis, University of Illinois at Urbana-Champaign (2003).
- [58] N. A. Zarkevich, E. H. Majzoub, and D. D. Johnson, Phys. Rev. B **89**, 134308 (2014).
- [59] M. R. Ibarra and P. A. Algarabel, Phys. Rev. B **50**, 4196 (1994).
- [60] N.A. Zarkevich, “Thermophonon code,” http://lib.dr.iastate.edu/ameslab_software/2/ (2014).
- [61] G. Kresse and J. Hafner, Phys. Rev. B **47**, RC558 (1993).
- [62] G. Kresse, and J. Hafner, Phys. Rev. B **49**, 14251 (1994).
- [63] N. A. Zarkevich and D. D. Johnson, J. Chem. Phys. **142**, 024106 (2015).
- [64] N. A. Zarkevich and D. D. Johnson, “C2NEB source code,” http://lib.dr.iastate.edu/ameslab_software/1/ (2014).
- [65] P. E. Blöchl, Phys. Rev. B **50**, 17953 (1994).
- [66] G. Kresse, and D. Joubert, Phys. Rev. B **59**, 1758 (1999).
- [67] J. P. Perdew, K. Burke, and M. Ernzerhof, Phys. Rev. Lett. **77**, 3865 (1996).
- [68] S. H. Vosko, L. Wilk, and M. Nusair, Can. J. Phys. **58**, 1200 (1980).
- [69] D. D. Johnson, Phys. Rev. B **38**, 12807 (1988).
- [70] H. J. Monkhorst and J. D. Pack, Phys. Rev. B **13**, 5188 (1976).